Paul Scherrer Institut

From the SelectedWorks of Dr. Et-touhami Es-sebbar

Winter May 4, 2014

Measurement of the Rate of Hydrogen Peroxide Thermal Decomposition in a Shock Tube Using Quantum Cascade Laser Absorption Near 7.7 μm

M. B. Sajid
Et. Es-sebbar
T. Javed
C. Fittschen
A. Farooq

Available at: http://works.bepress.com/et-touhami_es-sebbar/52/

Measurement of the Rate of Hydrogen Peroxide Thermal Decomposition in a Shock Tube Using Quantum Cascade Laser Absorption Near 7.7 μm

M. B. SAJID,[1] ET. ES-SEBBAR,[1] T. JAVED,[1] C. FITTSCHEN,[2] A. FAROOQ[1]

[1]*Clean Combustion Research Center, Division of Physical Sciences and Engineering, King Abdullah University of Science and Technology, Thuwal 23955–6900, Saudi Arabia*

[2]PC2A, *University Lille* 1, CNRS, *Cité Scientifique*, Bât. C11, 59655, *Villeneuve d'Ascq*, *France*

Received 27 July 2013; revised 17 September 2013; accepted 23 September 2013

DOI 10.1002/kin.20827
Published online 24 October 2013 in Wiley Online Library (wileyonlinelibrary.com).

ABSTRACT: Hydrogen peroxide (H_2O_2) is formed during hydrocarbon combustion and controls the system reactivity under intermediate temperature conditions. Here, we measured the rate of hydrogen peroxide decomposition behind reflected shock waves using midinfrared absorption of H_2O_2 near 7.7 μm. We performed the experiments in diluted H_2O_2/Ar mixtures between 930 and 1235 K and at three different pressures (1, 2, and 10 atm). Under these conditions, the decay of hydrogen peroxide is sensitive only to the decomposition reaction rate, $H_2O_2 + M \rightarrow 2OH + M$ (k_1). The second-order rate coefficient at low pressures (1 and 2 atm) did not exhibit any pressure dependence, suggesting that the reaction was in the low-pressure limit. The rate data measured at 10 atm exhibited falloff behavior. The measured decomposition rates can be expressed in Arrhenius forms as follows:

$$k_1(1 \text{ and } 2 \text{ atm}) = 10^{(16.29\pm0.12)} \times \exp(-21993 \pm 301/T) \qquad (\text{cm}^3\text{mol}^{-1}\text{s}^{-1})$$

$$k_1(10 \text{ atm}) = 10^{(15.24\pm0.10)} \times \exp(-19955 \pm 247/T) \quad (\text{cm}^3\text{mol}^{-1}\text{s}^{-1})$$

© 2013 Wiley Periodicals, Inc. Int J Chem Kinet 46: 275–284, 2014

Correspondence to: A. Farooq; e-mail: aamir.farooq@kaust.edu.sa.
© 2013 Wiley Periodicals, Inc.

INTRODUCTION

Modeling of the chemistry of combustion systems requires a large database of reaction coefficients including several critical reaction coefficients over a wide range of temperatures and pressures. Hydrogen peroxide (H_2O_2) is an important intermediate species that can be formed in high concentrations in such combustion systems [1–4]. The thermal decomposition of hydrogen peroxide, in the presence of a second body (M), results in highly reactive OH radicals, as indicated by the following reaction:

$$H_2O_2 + M \rightarrow 2\ OH + M \quad (k_1) \qquad (1)$$

This reaction controls the overall reactivity of the system in the intermediate temperature range (900–1200 K) [1] and plays a critical role in the operation of homogeneous charged, compression ignition (HCCI) engines, ignition processes in diesel engines, and knocking in spark ignition engines [2].

Several studies of the thermal decomposition of hydrogen peroxide were conducted in flow systems and static cells [5–9]. These studies were generally carried out below 900 K and hence provided limited information directly relevant to combustion applications. Despite the importance of this reaction, until now only two research groups (University of Göttingen, Germany, and Stanford University, Stanford, CA) studied the decomposition of H_2O_2 under combustion conditions using shock tube facilities. In 1969, the Göttingen group [10] obtained the first H_2O_2 decomposition rates behind reflected and incident shock waves between 950 and 1450 K and pressures up to 20 atm by using UV absorption spectroscopy at 230 and 290 nm. The Göttingen group studied the reaction again in 2002: Kappel et al. [11] studied the thermal decomposition of H_2O_2 behind reflected shock waves using UV absorption at 215, 230, and 290 nm. The rate coefficients were measured between 950 and 1235 K and at pressures of 1, 4, and 15 atm. However, the HO_2 interference at 215/230 nm and the relatively low H_2O_2 absorption at 290 nm affected the accuracy of these measurements somewhat [12]. Recently, Hong et al. [13], at Stanford University, measured H_2O_2 decomposition rates by using infrared (IR) absorption spectroscopy of H_2O near 2.55 μm, because the water formation rate is predominantly controlled by H_2O_2 decomposition. In their measurements, the decomposition rate of H_2O_2, in the presence of Ar and N_2 bath gases, was studied over the intermediate temperature range from 1000 to 1200 K and at relatively low pressures between 0.9 and 3.2 atm. Hong et al. [14] later combined UV absorption of OH (306.7 nm) and IR absorption of H_2O (2.55 μm) to remeasure the H_2O_2 decomposition rate and the H_2O_2 + OH reaction rate between 1020 and 1460 K and at pressure 1.8 atm.

The reverse recombination reaction (OH + OH) has also been investigated experimentally by flash photolysis of OH precursors to produce OH radials [15–18]. Trainer and von Rosenberg [15] performed experiments at room temperature and subatmospheric pressure. Zellner et al. [16] studied the reverse recombination reaction in the temperature range of 253–353 K and at pressures ranging from 26 to 1100 mbar. High-pressure measurements were carried out by Forster et al. [17] and Fulle et al. [18] at pressures up to 150 bar and temperatures up to 700 K. These measurements were complicated due to secondary reactions of OH radicals, and hence the measured rate varied by up to a factor of three in these studies. Recently, Sangwan et al. [19] measured the OH + OH rate using UV–vis absorption spectroscopy between 298 and 834 K and at pressures ranging from 1 to 100 bar with a stated uncertainty of ±21%.

Theoretical studies have also been conducted to determine the reaction rate of the thermal decomposition of hydrogen peroxide. Brouwer et al. [20] calculated the falloff curves and reaction rates in the temperature range of 200–1500 K using detailed and simplified statistical adiabatic channel models. Troe and Ushakov [21] performed ab initio calculations to study both dissociation and recombination reactions up to 5000 K and also predicted the falloff behaviors. Sellevåg et al. [22] used variable reaction coordinate transition state theory, classical trajectory simulations, and a two-transition-state model to report the low- and high-pressure limiting rate coefficients in the temperature range of 200–3000 K with He and Ar as bath gases. Troe [23] analyzed results from theoretical and experimental studies to determine the temperature and pressure dependence of thermal dissociation and recombination reactions of H_2O_2.

Accurate H_2O_2 decomposition rate coefficient measurements in a wide range of temperatures and pressures under combustion conditions are essential for predictive kinetic mechanisms. In the current work, we used tunable quantum cascade laser (QCL) absorption near 7.7 μm to determine the reaction rate of H_2O_2 decomposition behind reflected shock waves for temperatures ranging from 930 to 1250 K and at pressures of 1, 2, and 10 atm. The measurements were performed at a relatively low H_2O_2 concentration, diluted in Ar, to minimize the effect of secondary reactions and post-shock temperature rise.

EXPERIMENTAL

Shock Tube Facility

Hydrogen peroxide decomposition rate measurements were performed in a helium-driven, electro-polished, shock tube made of 304 stainless steel. The shock tube has an inner diameter of 14 cm and a driver section length of 9 m. The driver section length can be varied up to a maximum of 9 m. Test times up to 50 ms can be achieved by using contact surface tailoring [24,25] in different driver gas mixtures. In this study, the driver section has a length of 4.5 m and highly pure helium (99.99%) gas was used as the driver gas. The driven section was connected to mechanical and turbo pumps to achieve an ultimate pressure of about 10^{-6} Torr with an outgassing rate of 10^{-5} Torr min^{-1} with overnight pumping. A high accuracy Baratron pressure transducer was used to measure the preshock mixture pressure in the shock tube. Five PCB 113B26 piezoelectric pressure transducers (PZTs) connected to four ultrafast frequency counter/timers (350 MHz; Agilent 53220A) were employed to obtain the axial incident velocity profile. The incident shock velocity at the end wall of the driven section was determined by a linear extrapolation of the velocity profile. The velocity attenuation rates were less than 0.8% per meter, and the percentage error in calculated end-wall shock velocity varied between 0.07% and 0.2%. The reflected shock conditions, including pressure and temperature, were calculated by using one-dimensional shock jump equations. The thermodynamic parameters were taken from the Sandia thermodynamic database [26]. A PZT pressure transducer (Kistler 603B1) located at 2 cm from the end wall was used to monitor the sidewall pressure history; typical pressure trace is shown in Fig. 1 with a test time of approximately 3 ms. The postshock pressure variation with time (dP_5/dt) is approximately 2% per ms.

H_2O_2 Source and Delivery

Hydrogen peroxide is a very unstable species, and it can decompose rapidly on the surfaces with which it comes in contact. Owing to its instability, high concentrations of H_2O_2 solutions are not supplied and generally 30%–50% aqueous solutions containing trace amounts of ethylenediaminetetraacetic acid for stabilization are commercially available. As the vapor pressure of H_2O_2 is significantly smaller than that of water, diluted solutions cannot be used to obtain pure H_2O_2 vapors. Although there is no simple precursor of H_2O_2, commercially available urea–H_2O_2 adduct has been used upon gentle heating to obtain relatively pure

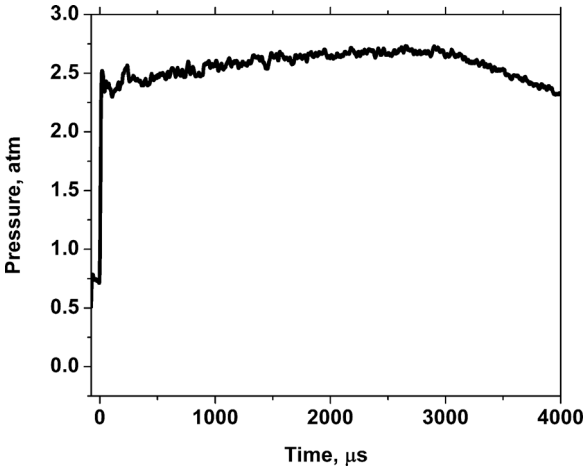

Figure 1 Typical pressure trace during a H_2O_2 decomposition rate measurement. The test conditions were $T_5 =$ 1167 K, $P_5 = 2.35$ atm, with argon used as the bath gas.

H_2O_2 vapor [13,27]. However, the presence of small amounts of water vapor was still reported [13]. Here, we started off with 50% H_2O_2 aqueous solution and converted it to a high-concentration H_2O_2 solution by continuously bubbling argon gas and vacuuming the mixture. Figure 2 shows the schematic of the H_2O_2 delivery system into the driven section of the shock tube. As water has a higher vapor pressure than hydrogen peroxide, 23.8 Torr compared with 1.98 Torr, at 298 K [28], bubbling and vacuuming processes removed more water from the aqueous H_2O_2 solution. The vapor pressure of the mixture was monitored by using a highly accurate Baratron pressure transducer. An empty container was placed between the mass flow controller and the container for the H_2O_2 solution to avoid accidental back flow up to the flow controller. To reduce the decomposition of H_2O_2 on surfaces, tubes and valves made of Teflon or stainless steel were used.

The mixture used for the shock tube experiments had a total vapor pressure of approximately 2.3 Torr. To introduce the H_2O_2/Ar mixture in the shock tube, the vacuum pump was isolated and the stream containing the H_2O_2/Ar mixture was further diluted by a separate flow of argon. This procedure helped in minimizing the water concentration and in controlling the mole fraction of H_2O_2 in the initial (preshock) mixture. A flow rate of 700 sccm of Ar for both streams was used to obtain approximately 0.4%–0.5% H_2O_2 in the initial mixture.

Optical Diagnostic Setup

A continuous wave external cavity quantum cascade laser (cw EC-QCL) provided by Daylight Solutions

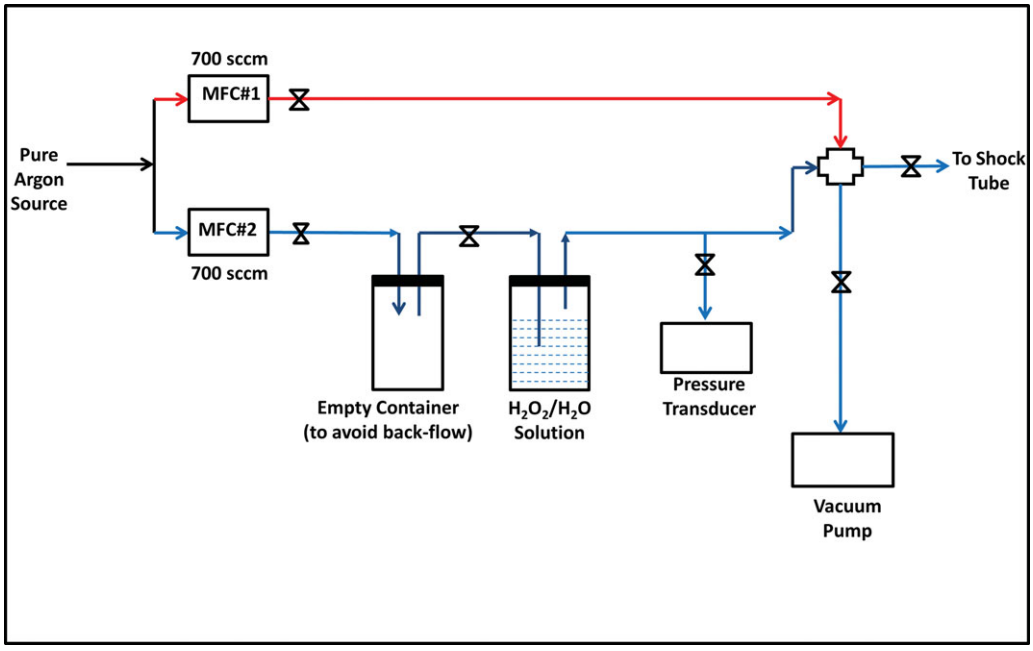

Figure 2 Schematic of the H_2O_2 delivery system from a H_2O_2/H_2O solution.

was used in this study. The laser (21077-MHF) has a tunable range of 1217–1328 cm^{-1} and covers the strongest spectroscopic features of H_2O_2 near 7.7 μm. The laser head was connected to a controller system that displayed the laser frequency and was used to set the laser voltage, current, and laser scan mode. The laser can be finely tuned to different wavelengths by adjusting the laser frequency, temperature, and injection current to the laser head. Depending on the nature of the application, the laser can be operated in three different modes: fixed wavelength, coarse modulation, and high-frequency modulation. High-frequency modulation provides a tuning range of approximately 0.1 cm^{-1} at frequencies ranging from 10 kHz to 2 MHz. Coarse modulation provides a wider tuning range of nearly 1 cm^{-1} at a maximum frequency of 100 Hz. Coarse modulation was achieved by using a PZT installed in the cw (continuous mode) mode hop free (MHF) drive train of the laser, which mechanically modulated the grating. The PZT was driven by an external piezo-driver (Thorlabs MDT694A), which received sine waves generated by a standard function generator (Stanford Research Systems; DS 345). The IR radiation output was highly collimated with sufficient power (>120 mW), and the specified line width of the laser was less than 0.001 cm^{-1}.

Figure 3 shows a schematic of the optical setup used in the current study. The IR light from the cw EC-QCL was transmitted through GaAs windows located at an axial location 2 cm from the shock tube end wall. To control the beam steering, an iris was placed upstream of the shock tube to reduce the beam size. A second iris was placed downstream of the shock tube to minimize thermal emissions originating from the shock tube. Common mode rejection [29] was employed by using a reference detector to minimize the effect of laser noise on the absorption signal. The laser intensity was measured with thermoelectrically cooled, optically immersed photovoltaic detectors (Vigo PVI 3TE-10.6). A germanium etalon, with a free spectral range of 0.0163 cm^{-1}, was used to measure the wavelength tuning in the coarse modulation mode. The laser intensity and Kistler pressure transducer signals were recorded by a National Instruments data acquisition system (NI PCI-6133 DAQ) with a sampling rate of 2.5 MS s^{-1}. A custom-built LabView program was used to record the data.

INTERFERENCE-FREE H_2O_2 DIAGNOSTIC

As shown in Fig. 4, H_2O_2 molecules absorb across several wavelength regions in the IR [28]. The strongest absorption features occur at around 7.7 μm, i.e., 1200–1350 cm^{-1}, and were accessible by our laser system. However, water vapor also absorbs strongly across the same wavelength region, and there are only narrow absorption regions for H_2O_2 that are free from interference from H_2O. We used spectral simulations on

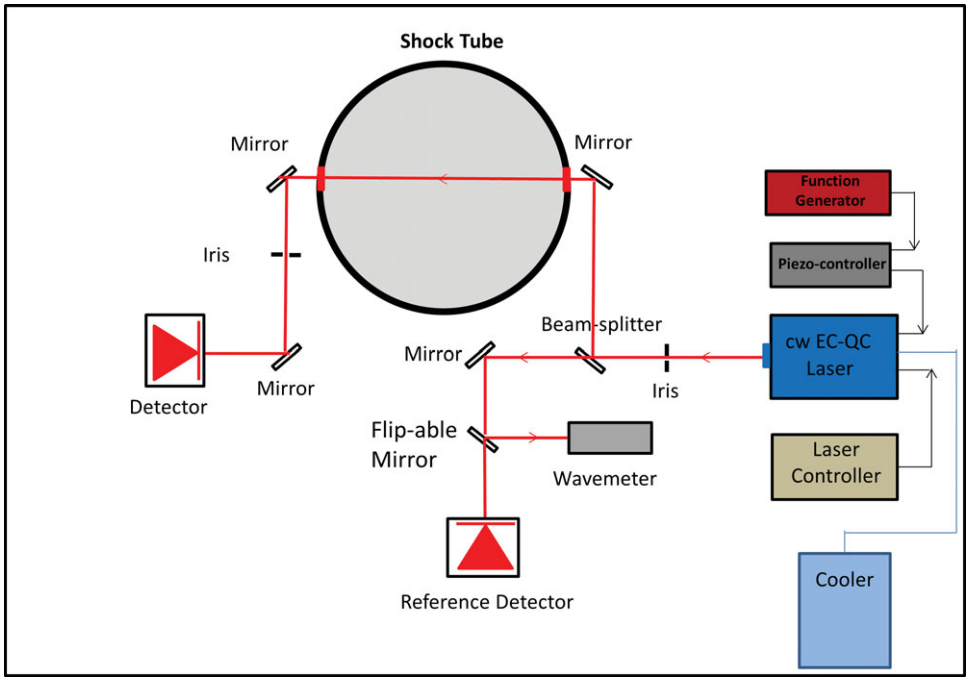

Figure 3 Overview of the experimental setup.

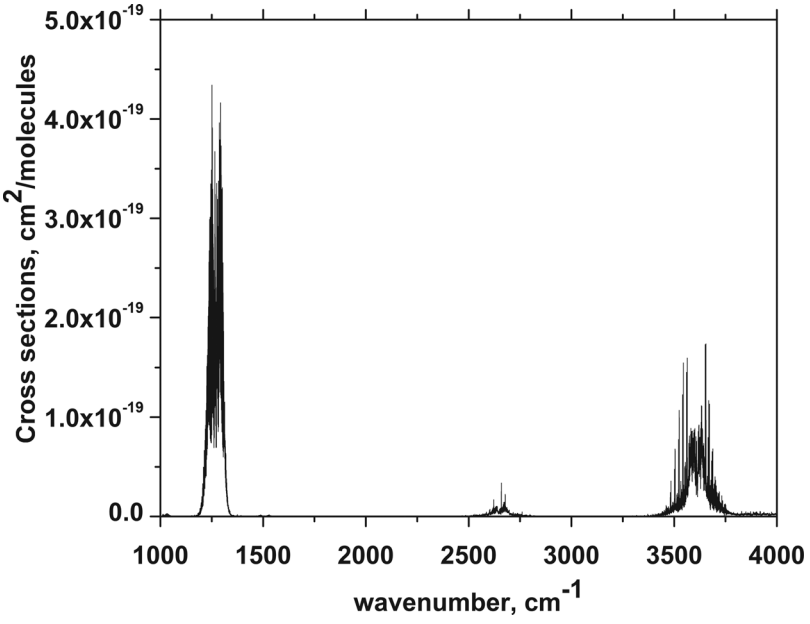

Figure 4 Room temperature (296 K) IR cross sections of hydrogen peroxide from 1000 to 4000 cm^{-1} (from the PNNL database [28]).

water vapor and hydrogen peroxide to identify the optimal H_2O_2 transition—that is, the highest absorption strength and the least interference from H_2O—for the expected conditions of our experiment. These simulations are shown in Fig. 5a and are based on the HITRAN 2008 database [30]. Figure 5b shows the selected H_2O_2 spectral feature around 1302 cm^{-1}, which is sufficiently strong and has minimum interference from water. This feature was used in the fixed wavelength measurements of the H_2O_2 time history during

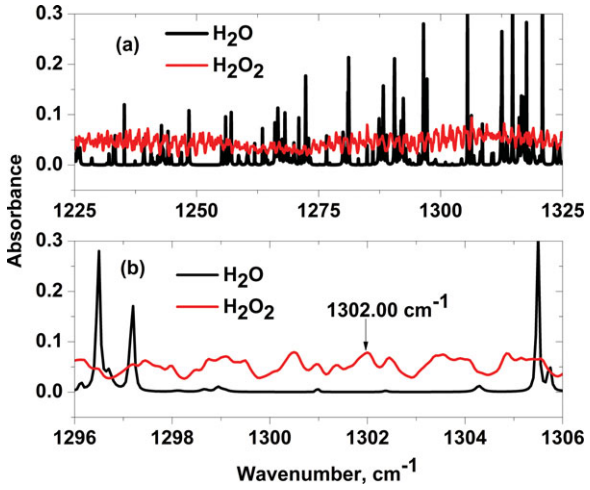

Figure 5 (a) Spectrum simulation of H_2O_2 and H_2O across the tuning range of our laser; (b) zoomed-in view of the spectral region near 1302 cm^{-1} used to measure the H_2O_2 molar fraction. The test conditions were $T = 1000$ K, $P = 2.5$ atm, $X_{H2O2} = 0.45\%$, $X_{H2O} = 0.5\%$, $L = 14$ cm.

the reflected shock wave experiments. The frequency of the laser was monitored by a wavelength meter (Bristol Instruments 721).

The initial H_2O_2 mole fraction in the mixture loaded into the driven section of the shock tube was determined by scanning the laser across the H_2O_2 line at 1302.5119 cm^{-1} (Fig. 6a). As there were several H_2O_2 absorption lines within a single scan (~1 cm^{-1}) of the laser, a C_2H_2 transition near 1302.59 cm^{-1} was used to identify the targeted H_2O_2 line. This was achieved by loading 1% C_2H_2/Ar mixture at 1 Torr into the shock tube and then scanning the laser in the coarse modulation mode to record the acetylene transition at 1302.59 cm^{-1}. We then vacuumed the driven section of the shock tube with a turbomolecular pump to ensure that no C_2H_2 remained in the system. In the H_2O_2 measurements, the reference signal (I_0) and etalon trace were recorded with the shock tube under a vacuum. Thereafter, the H_2O_2/Ar mixture was injected in the shock tube and the transmitted signal (I_t) was recorded at the initial shock fill pressure (P_1). The measured absorbance was then calculated using the Beer–Lambert relation: $\ln(I_0/I_t) = P_1 X_{H_2O_2} L\phi(\nu)S(T)$, where L is the laser path length (14 cm) through the shock tube, $\phi(\nu)$ is the lineshape function expressed in centimeters, $S(T)$ is the line strength of the H_2O_2 transition expressed in cm^{-2} atm^{-1} taken from the HITRAN spectral database [30], and $X_{H_2O_2}$ is the molar fraction of H_2O_2. The room temperature line strength values listed in the HITRAN database have an uncertainty of 5%–10%. The derived absorbance was fitted to the Voigt profile to obtain the integrated area (Fig. 6b), which was used to determine the mole fraction of H_2O_2

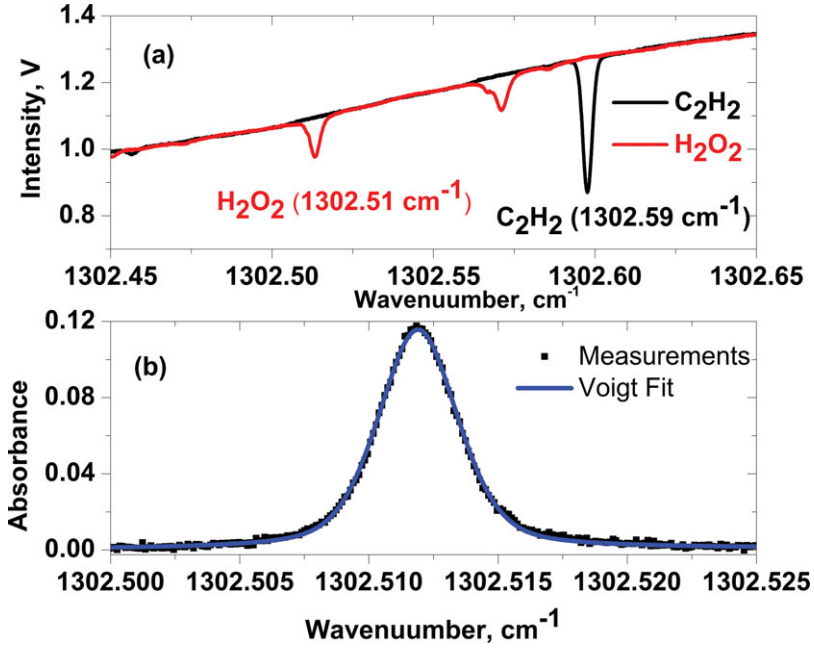

Figure 6 (a) Laser modulation around 1302 cm^{-1} for measuring the initial H_2O_2 molar fraction. A line of C_2H_2 at 1302.59 cm^{-1} was used to identify the H_2O_2 lines; (b) resulting H_2O_2 absorbance (square symbols), fitted with a Vogit profile (solid line). The test conditions were 9.8 Torr, 296 K, and 14 cm path length. The resulting H_2O_2 molar fraction is 0.42% in this case.

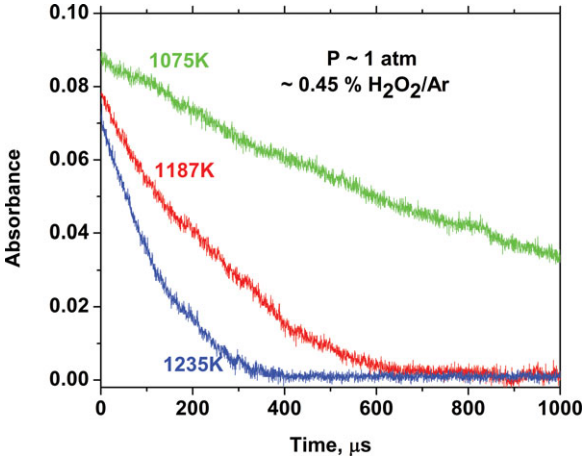

Figure 7 Absorption signals for H_2O_2 decay at different temperatures for measurements near 1 atm.

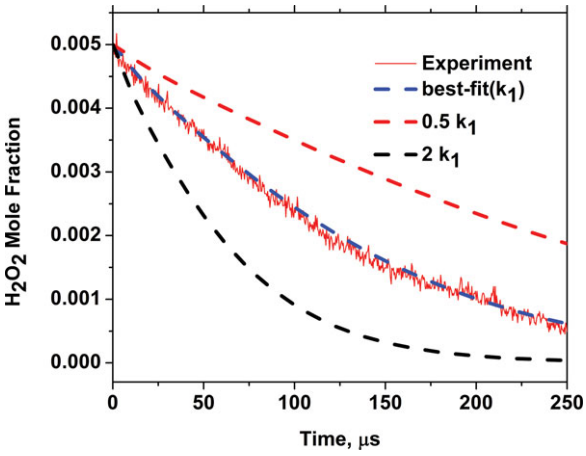

Figure 8 The H_2O_2 molar fraction time history for reflected shock conditions of $T = 1167$ K, $P = 2.35$ atm, $X_{H_2O_2} = 0.5\%$, and $X_{H_2O} = 0.4\%$ in Ar bath gas. The best-fit result is $k_1 = 1.45 \times 10^8$ cm^{3}mol^{-1} s^{-1}. Decay profiles with $2k_1$ and $0.5k_1$ are also plotted. The simulated profiles are not affected by $\pm 10\%$ variation in X_{H_2O}.

in the initial mixture. The mole fraction of water vapor in the gas-phase mixture was calculated by applying Raoult's law. Furthermore, an H_2O absorption diagnostic near 2.8 μm was used to confirm the very small levels of water vapor (~0.4%–0.5%) present in the initial mixture.

After we measured the initial H_2O_2 mole fraction, we switched the laser to the fixed wavelength mode to measure the decay of H_2O_2 in the postshock region. We then used the absorbance value at time zero (after the reflected shock) and the known initial (preshock) H_2O_2 mole fraction to calculate the H_2O_2 absorption cross section for each shock. We could thus convert the measured H_2O_2 absorbance time histories to absolute molar fraction values.

RESULTS AND DISCUSSION

In this study, we measured the reaction rate (k_1) of the thermal decomposition of hydrogen peroxide, diluted with Ar, behind reflected shock waves in a shock tube. We conducted the experiments at temperatures between 930 and 1250 K and pressures of 1, 2, and 10 atm. Figure 7 shows a few representative absorption time histories of H_2O_2 decomposition across a range of temperatures and at a pressure of about 1 atm. The decay of H_2O_2 is strongly dependent on temperature, and the decay rate increases significantly with as the temperature increases. Furthermore, the initial absorbance of H_2O_2 decreases as the temperature increases due to the relatively low value of the lower state energy (E'') of the selected H_2O_2 absorption transition.

Figure 8 presents an example of the H_2O_2 molar fraction time history derived from absorption measurements at a postshock temperature of 1167 K and a pressure of 2.35 atm. The initial H_2O_2 mole fraction was 0.50% in the example shown in Fig. 8, but it varied between 0.4% and 0.5% in other cases. To extract the rate constant, k_1, we fitted the experimental decays using the H_2/O_2 mechanism, such as described by Hong et al. [31]. Under the conditions of Fig. 8, the best fit to our experimental data correlated with a rate constant of 1.45×10^8 cm^3 mol^{-1} s^{-1}. To demonstrate the sensitivity of H_2O_2 profiles to the decomposition rate constant, we ran simulations, also presented in Fig. 8, in which the best-fit k_1 was varied to $2k_1$ and $0.5k_1$. We also confirmed that the sensitivity of the H_2O_2 decays to the rate constant, k_1, by sensitivity analysis (Fig. 9): the sensitivity, $\alpha_{i-H_2O_2}(t)$, is defined [13] here as the partial derivative of the H_2O_2 mole fraction ($X_{H_2O_2}$) with respect to the rate constant of a reaction ($A_{\downarrow}i$), normalized by the maximum H_2O_2 mole fraction and the rate constant parameter, i.e.,

$$\alpha_{i-H_2O_2}(t) = \frac{\frac{dX_{H_2O_2}}{X^{max}_{H_2O_2}}}{\frac{dA_i}{A_i}} \tag{2}$$

In Fig. 10, we plot the second-order H_2O_2 decomposition rates as a function of $1000/T$ for the three pressures considered here, 1, 2, and 10 atm. As indicated in the figure, the rate constants of pressure-dependent reactions do not change with pressure as long as the reaction is within the low-pressure limit; at pressures for which the reaction is in the falloff region, the rate constants decrease with increasing pressure. As can be seen in Fig. 10, the H_2O_2 reaction rates at relatively

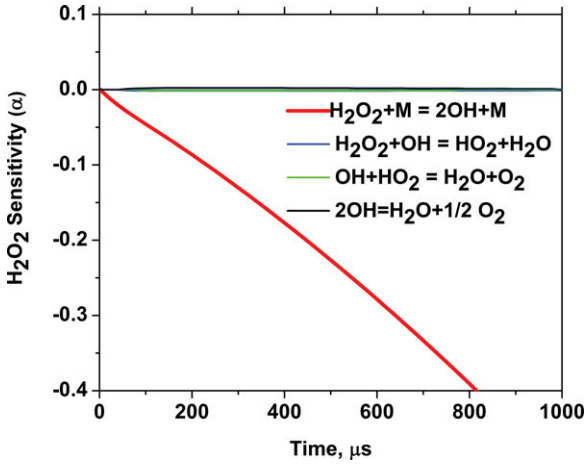

Figure 9 Sensitivity analysis of H_2O_2 decay using Hong et al.'s [31] mechanism at typical postshock conditions: $T =$ 1000 K, $P = 2.5$ atm, $X_{H_2O_2} = 0.45\%$, and $X_{H_2O} = 0.5\%$ in Ar.

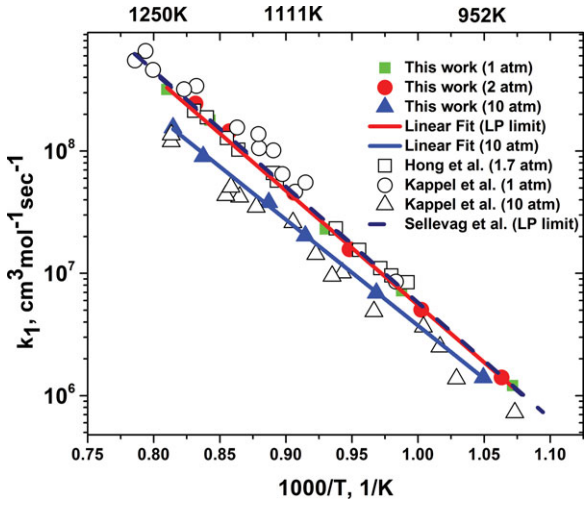

Figure 10 H_2O_2 rate coefficients measured as a function of temperature at three pressures (1, 2, and 10 atm). Best-fit Arrhenius curves for low (1 and 2 atm) and high pressure (10 atm) are also shown. Comparisons with previous measurements and theoretical calculations are also shown.

low-pressure values, 1 and 2 atm, exhibit negligible pressure dependence between 930 and 1250 K, implying that the reaction is within the low-pressure limit at these pressures. Measurements of the second-order rate constant at 10 atm are lower compared with those at 1 and 2 atm, demonstrating that the reaction is in the falloff regime at 10 atm. As an example, the second-order rate constant decreases by about 50% at 1100 K when the pressure is increased from 2 to 10 atm. The measured second-order rate constant and pseudo–first-order rate constant results are listed in Table I. Owing

Table I Measured Reaction Rates and Experimental Conditions

P (atm)	T (K)	Initial H_2O_2 (%)	k_1 (cm^3 mol^{-1} s^{-1})	k_1*[Ar] (s^{-1})
1.18	933.3	0.44	1.21E+06	1.86E+01
1.15	1012.5	0.42	7.20E+06	9.93E+01
1.13	1075.4	0.43	2.30E+07	2.94E+02
1.08	1186.8	0.45	1.78E+08	1.97E+03
1.03	1234.6	0.46	3.19E+08	3.23E+03
2.25	940.5	0.44	1.41E+06	4.10E+01
2.33	997.54	0.47	5.04E+06	1.43E+02
2.31	1054.7	0.46	1.57E+07	4.18E+02
2.37	1103.5	0.47	4.55E+07	1.19E+03
2.35	1166.6	0.50	1.45E+08	3.55E+03
2.29	1202.4	0.48	2.45E+08	5.67E+03
10.17	952.9	0.46	1.40E+06	1.82E+02
10.08	1032.6	0.45	6.89E+06	8.17E+02
10.13	1093.3	0.48	2.03E+07	2.28E+03
10.10	1127.4	0.46	3.80E+07	4.14E+03
10.06	1194.2	0.45	9.02E+07	9.23E+03
9.95	1227.6	0.48	1.55E+08	1.53E+04

to the falloff behavior, the activation energies in the low-pressure limit (1 and 2 atm) and at 10 atm are slightly different. Kappel et al. [11] observed similar behavior in their experimental study.

We fitted our measurements on the basis of Arrhenius's equation in the temperature range of 930–1250 K. We found the best-fit rates for the low-pressure limit (1 and 2 atm) and at 10 atm to be

$$k_1(1 \text{ and } 2 \text{ atm}) = 10^{(16.29\pm0.12)} \times \exp(-21{,}993 \pm 301/T) \quad (\text{cm}^3\text{mol}^{-1}\text{s}^{-1}) \tag{3}$$

$$k_1(10 \text{ atm}) = 10^{(15.24\pm0.10)} \times \exp(-19{,}955 \pm 247/T) \quad (\text{cm}^3\text{mol}^{-1}\text{s}^{-1}) \tag{4}$$

These best-fit rates and comparisons with previous measurements are also presented in Fig. 10. Our data agree very well with the measurements by Kappel et al. [11] and Hong et al. [13] even though these two experimental studies used different diagnostics compared to the method we used. There is also a good agreement between our low-pressure measurements and the theoretical calculations by Sellevag et al. [22] for the low-pressure limit.

Figure 11 shows the falloff behavior of the rate constant of the decomposition of H_2O_2. The pseudo–first-order rate is plotted as a function of the concentration

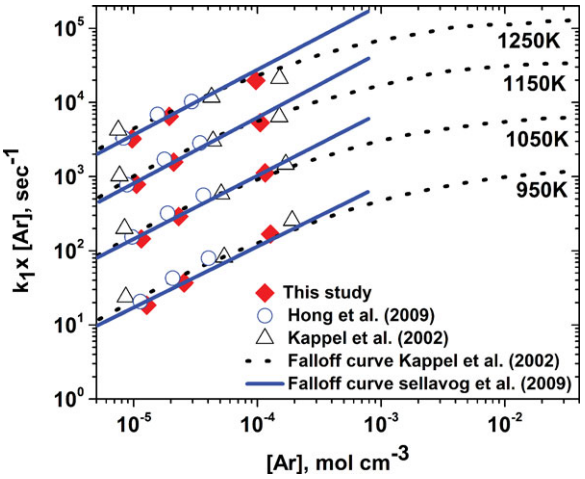

Figure 11 The falloff behavior of the H_2O_2 decomposition rate in an Ar bath gas. Comparisons with previous measurements and calculations are also shown.

of the Ar bath gas at four temperatures. Data points for experimental studies are obtained from the rate expressions at specific pressures, i.e., Eqs. (3) and (4) in our study. Comparisons with Kappel et al.'s [11] proposed falloff curves and Sellevag et al.'s [22] calculated falloff curves near the low-pressure limit are shown. We note that the experimental data are available only near the low-pressure limit, and there are few experimental data available for the high-pressure limit of k_1. Kappel et al. [11] developed falloff curves based on their measurements at pressures of 1, 4, and 15 atm. However, uncertainty exists in these falloff curves due to the scatter in their experimental data and to the unavailability of data near the high-pressure limit.

Troe and Ushakov [21] theoretically calculated the rate constant in the high-pressure limit based on reverse recombination reaction measurements performed at room temperature and at a very high pressure of 150 bar. Comparisons of the measurements of Kappel et al. [11] with the calculations of Troe and Ushakov [21] show earlier deviation from the low-pressure limit than predicted by the theoretical calculations. Sellevag et al. [22] calculated the falloff curves for the studied reaction near the low-pressure limit by using a two-dimensional master equation. They used the energy transfer parameters obtained from Kappel et al.'s [11] measurements. However, they observed that these measurements showed earlier deviation from low-pressure limit than predicted by their calculations. Our measurements at 10 atm also show the deviation from the second-order behavior. Direct measurements at much higher pressures are needed to improve the evaluation of the falloff behavior of this reaction.

The primary sources of uncertainty in our determination of the rate constant, k_1, come from (i) the determination of the postshock gas temperature, (ii) the H_2O_2 mole fraction in the initial mixture loaded in the shock tube, and (iii) the fitting procedure of the measured H_2O_2 time histories. The uncertainty in the postshock temperature varies from 0.65% at 1234 K to 0.75% at 933 K, as evaluated from the error in the velocity calculation, the extrapolation of velocity to the end wall, and the temperature change due to dP_5/dt. The longer times needed to fit the slow decay of H_2O_2 at low temperatures result in larger temperature uncertainty (0.75%). The temperature uncertainty results in 12%–20% uncertainty in the rate constant measurement from high to low temperatures. The uncertainty in the calculation of postshock pressure is about 2% and has very little effect on the rate calculation. The uncertainty in the initial mixture composition is estimated to be less than 10%, which results in a nearly 5% uncertainty in the determination of the rate constant due to the changing importance of the secondary reactions in the H_2/O_2 mechanism. The error in the fitting procedure due to uncertainties in the rate constants of different reactions in the H_2/O_2 mechanism results in an approximately 5% uncertainty in the rate constant. By combining all these uncertainties in a root-sum-squares method, the overall uncertainty in the determination of the k_1 reaction rate is estimated to be 14% at 1234 K and 21% at 933 K.

CONCLUSIONS

In this study, we investigated the decomposition of H_2O_2 molecules in the presence of Ar bath gas behind reflected shock waves using quantum cascade laser absorption near 7.7 μm. Reaction rates were measured in the temperature range of 930–1250 K and at three pressures, 1, 2, and 10 atm. Our results show that the rate constant for H_2O_2 decomposition is within the low-pressure limit at 1 and 2 atm and is in the falloff regime at 10 atm. The measured data can be represented with the following Arrhenius equations:

$$k_1(1 \text{ and } 2 \text{ atm}) = 10^{(16.29\pm0.12)} \times \exp(-21{,}993 \pm 301/T) \quad (\text{cm}^3\text{mol}^{-1}\text{s}^{-1})$$

$$k_1(10 \text{ atm}) = 10^{(15.24\pm0.10)} \times \exp(-19{,}955 \pm 247/T) \quad (\text{cm}^3\text{mol}^{-1}\text{s}^{-1})$$

Further measurements at higher pressures are needed to ascertain better falloff curves and the

high-pressure limit for this important decomposition reaction.

We would like to acknowledge the funding provided by the Clean Combustion Research Center at King Abdullah University of Science and Technology, Thuwal, Saudi Arabia, and by Saudi Aramco under the FUELCOM program. Dr. Fittschen thanks the European Commission for funding through the Erasmus Mundus Gulf Countries Programme (EMA2-STRAND 2, LOT4).

BIBLIOGRAPHY

1. Bahrini, C.; Herbinet, O.; Glaude, P.-A.; Schoemaecker, C.; Fittschen, C.; Battin-Leclerc, F. J Am Chem Soc 2012, 134, 11944–11947.
2. Westbrook, C. K. Proc Combust Inst 2000, 28, 1563–1577.
3. Griffiths, J.; Hughes, K.; Porter, R. Proc Combust Inst 2005, 30, 1083–1091.
4. Aceves, S. M.; Flowers, D. L.; Martinez-Frias, J.; Smith, J. R.; Dibble, R.; Au, M.; Girard, J. SAE 2077, 2001.
5. Baldwin, R.; Brattan, D. In Symposium (International) on Combustion, 1961; pp. 110–119.
6. McLane, C. J Chem Phys 1949, 17, 379.
7. Satterfield, C. N.; Stein, T. W. J Phys Chem 1957, 61, 537–540.
8. Forst, W. Can J Chem 1958, 36, 1308–1319.
9. Hoare, D.; Protheroe, J.; Walsh, A. Trans Faraday Soc 1959, 55, 548–557.
10. Meyer, E.; Olschewski, H.; Troe, J.; Wagner, H. G. In Symposium (International) on Combustion, 1969; pp. 345–355.
11. Kappel, C.; Luther, K.; Troe, J. Phys Chem Chem Phys 2002, 4, 4392–4398.
12. Kijewski, H.; Troe, J. Helv Chim Acta 1972, 55, 205–213.
13. Hong, Z.; Farooq, A.; Barbour, E. A.; Davidson, D. F.; Hanson, R. K. J Phys Chem A 2009, 113, 12919–12925.
14. Hong, Z.; Cook, R. D.; Davidson, D. F.; Hanson, R. K. J Phys Chem A 2010, 114, 5718–5727.
15. Trainor, D. W.; von Rosenberg, C, Jr. J Chem Phys 1974, 61, 1010.
16. Zellner, R.; Ewig, F.; Paschke, R.; Wagner, G. J Phys Chem 1988, 92, 4184–4190.
17. Forster, R.; Frost, M.; Fulle, D.; Hamann, H.; Hippler, H.; Schlepegrell, A.; Troe, J. J Chem Phys 1995, 103, 2949.
18. Fulle, D.; Hamann, H.; Hippler, H.; Troe, J. J Chem Phys 1996, 105, 1001.
19. Sangwan, M.; Chesnokov, E. N.; Krasnoperov, L. N. J Phys Chem A 2012, 116, 6282–6294.
20. Brouwer, L.; Cobos, C.; Troe, J.; Dübal, H. R.; Crim, F. J Chem Phys 1987, 86, 6171.
21. Troe, J.; Ushakov, V. Phys Chem Chem Phys 2008, 10, 3915–3924.
22. Sellevåg, S. R.; Georgievskii, Y.; Miller, J. A. J Phys Chem A 2009, 113, 4457–4467.
23. Troe, J. Combust Flame 2011, 158, 594–601.
24. Hong, Z.; Davidson, D. F.; Hanson, R. K. Shock Waves 2009, 19, 331–336.
25. Amadio, A. R.; Crofton, M. W.; Petersen, E. L. Shock Waves 2006, 16, 157–165.
26. Kee, R.; Rupley, F.; Miller, J. SAND87–8215B; UC-4, Sandia National Laboratory, Albuquerque, NM, 1987.
27. Ludwig, W.; Brandt, B.; Friedrichs, G.; Temps, F. J Phys Chem A 2006, 110, 3330–3337
28. Sharpe, S. W.; Johnson, T. J.; Sams, R. L.; Chu, P. M.; Rhoderick, G. C.; Johnson, P. A. Appl Spectrosc 2004, 58, 1452–1461.
29. Cook, R. D.; Pyun, S. H.; Cho, J.; Davidson, D. F.; Hanson, R. K. Combust Flame 2011, 158, 790–795.
30. Rothman, L. S.; Gordon, I. E.; Barbe, A.; Benner, D. C.; Bernath, P. F.; Birk, M.; Boudon, V.; Brown, L. R.; Campargue, A.; Champion, J.-P. J Quant Spectrosc Radiat Transfer 2009, 110, 533–572.
31. Hong, Z.; Davidson, D. F.; Hanson, R. K. Combust Flame 2011, 158, 633–644.